

TOPICAL REVIEW

Toward guiding principles for the design of biologically-integrated electrodes for the central nervous system

To cite this article: Cort H Thompson *et al* 2020 *J. Neural Eng.* **17** 021001

View the [article online](#) for updates and enhancements.



The Department of Bioengineering at the University of Pittsburgh Swanson School of Engineering invites applications from accomplished individuals with a PhD or equivalent degree in bioengineering, biomedical engineering, or closely related disciplines for an open-rank, tenured/tenure-stream faculty position. We wish to recruit an individual with strong research accomplishments in Translational Bioengineering (i.e., leveraging basic science and engineering knowledge to develop innovative, translatable solutions impacting clinical practice and healthcare), with preference given to research focus on neuro-technologies, imaging, cardiovascular devices, and biomimetic and biorobotic design. It is expected that this individual will complement our current strengths in biomechanics, bioimaging, molecular, cellular, and systems engineering, medical product engineering, neural engineering, and tissue engineering and regenerative medicine. In addition, candidates must be committed to contributing to high quality education of a diverse student body at both the undergraduate and graduate levels.

[CLICK HERE FOR FURTHER DETAILS](#)

To ensure full consideration, applications must be received by June 30, 2019. However, applications will be reviewed as they are received. Early submission is highly encouraged.



TOPICAL REVIEW

Toward guiding principles for the design of biologically-integrated electrodes for the central nervous system

RECEIVED
18 October 2019REVISED
31 December 2019ACCEPTED FOR PUBLICATION
27 January 2020PUBLISHED
12 March 2020Cort H Thompson¹, Ti'Air E Riggins¹, Paras R Patel², Cynthia A Chestek^{2,3,4,5}, Wen Li^{6,7} and Erin Purcell^{1,6,7}¹ Department of Biomedical Engineering, Michigan State University, East Lansing, MI, United States of America² Department of Biomedical Engineering, University of Michigan, Ann Arbor, MI, United States of America³ Department of Electrical Engineering and Computer Science, University of Michigan, Ann Arbor, MI, United States of America⁴ Neurosciences Program, University of Michigan, Ann Arbor, MI, United States of America⁵ Robotics Program, University of Michigan, Ann Arbor, MI, United States of America⁶ Department of Electrical and Computer Engineering, Michigan State University, East Lansing, MI, United States of America⁷ Institute for Quantitative Health Science and Engineering, Michigan State University, East Lansing, MI, United States of AmericaE-mail: epurcell@msu.edu**Keywords:** neural engineering, microelectrode array, gliosis, neuroprosthesis, biocompatibility, biological integration, neural interface designSupplementary material for this article is available [online](#)**Abstract**

Innovation in electrode design has produced a myriad of new and creative strategies for interfacing the nervous system with softer, less invasive, more broadly distributed sites with high spatial resolution. However, despite rapid growth in the use of implanted electrode arrays in research and clinical applications, there are no broadly accepted guiding principles for the design of biocompatible chronic recording interfaces in the central nervous system (CNS). Studies suggest that the architecture and flexibility of devices play important roles in determining effective tissue integration: device feature dimensions (varying from 'sub'- to 'supra'-cellular scales, $< 10 \mu\text{m}$ to $> 100 \mu\text{m}$), Young's modulus, and bending modulus have all been identified as key features of design. However, critical knowledge gaps remain in the field with respect to the underlying motivation for these designs: (1) a systematic study of the relationship between device design features (materials, architecture, flexibility), biointegration, and signal quality needs to be performed, including controls for interaction effects between design features, (2) benchmarks for success need to be determined (biological integration, recording performance, longevity, stability), and (3) user results, particularly those that champion a specific design or electrode modification, need to be replicated across laboratories. Finally, the ancillary effects of factors such as tethering, site impedance and insertion method need to be considered. Here, we briefly review observations to-date of device design effects on tissue integration and performance, and then highlight the need for comprehensive and systematic testing of these effects moving forward.

1. Introduction

Electrode arrays implanted in the brain have created a renaissance in the study of normal and pathological brain function. These devices are being developed to treat a growing number of medical conditions, including Parkinson's disease, paralysis, Alzheimer's disease, depression, Tourette's syndrome, deafness, blindness, stroke or tinnitus [1–20]. Many of these conditions are treated through electrical stimulation, where closed-loop systems can provide added therapeutic and performance benefits by conditioning

stimulation based on a recorded 'trigger' signal [21]. Recorded signals are also used to drive the decoding algorithms used to restore function for paralysis patients through brain-machine interfaces. While many successes in chronic recordings have been reported, these devices are characterized by an often variable ability to sense or stimulate activity over time [22–25]. This variability burdens decoding strategies and compromises the fidelity of closed-loop systems. The foreign body response to the implant is widely believed to be a key underlying source of signal instability and loss, where local neuronal loss and

encapsulation by a glial ‘scar’ progressively isolate devices from signal-generating neural circuitry [26,27]. Likewise, newer observations suggest that devices impact the function of the remaining neurons at the implanted interface [28–30], and implantation in motor cortex has produced behavioral deficits in rodents [31].

Despite these observations, direct, mechanistic links between specific cellular responses in the brain, device design features, and chronic performance remain to be established. Two central issues impede progress: (1) the relationship between the biological response to electrodes, and the impact on signal quality, is unclear, and (2) the surge in new electrode designs, which simultaneously alter multiple attributes of the array (materials, feature size, architecture), complicates the ability to assimilate observations across studies into guiding principles for electrode design. On the first issue, it remains unknown as to which aspects of the tissue response determine effective chronic performance. Local neuronal and glial densities are commonly used as metrics for assessing biocompatibility, but given the complexity of the system, these broad-based assessments may not provide the level of granularity necessary to identify key biomarkers of device performance. Brain cells are highly heterogeneous, where neurons can be distinguished based on unique structural and functional properties [32,33]. Likewise, non-neuronal cells are more complex than previously appreciated, and may respond to implanted electrode arrays in unexpected ways. For instance, recent evidence suggests that neuron glial antigen-2 (NG2)-glia react to device implantation within the initial days following insertion, exhibiting altered morphology and migration toward the interface [34]. Likewise, reactive astrocytes can be delineated into unique subclasses of phenotypes, with the potential to influence the structure and function of neural circuitry in distinct ways [35]. These cells can exert either positive or negative effects on surrounding neurons following injury [36], and a recent report distinguishes a pro-inflammatory, *neurotoxic* astroglial subtype from a hypoxia-induced, *neuroprotective* subtype [37]. Injury surrounding an electrode can produce differential effects on subtypes of neurons as well: shifts in the expression of excitatory and inhibitory synaptic transporters reportedly occur proximally to devices, indicating a progression toward increased inhibitory tone in the tissue surrounding chronically implanted electrodes [29]. Likewise, observations of sustained calcium influx and changes in the expression of voltage-gated ion channels indicate that implanted electrodes may alter the intrinsic excitability of the neurons they are designed to interface with [28,30], illustrating the potential for devices to not only affect cellular densities, but also the *function* of residual cells at the interface.

Regarding the second issue, recent years have seen a veritable explosion in the design strategies that characterize implanted electrode arrays. New devices

can feature a variety of architectures, dimensions, insertion strategies, materials, and modifications as they push the boundaries of neural interface design. However, the relationship between complex biological effects and the design attributes of the implanted electrode array remains undefined, even for relatively traditional designs and metrics of tissue response. Studies which directly and systematically test the effect of new design features *in isolation* on the biological response to implants are generally scarce, which is a problem compounded by the differing materials, bending stiffnesses, and feature sizes of recent ‘next-generation’ devices at the forefront of neural engineering research. As such, many of these devices utilize a wholly unique blend of characteristics that make it difficult to empirically determine which of the chosen features contribute to the observed tissue response. Furthermore, it is generally unclear whether or not any observed improvements in biocompatibility translate to improved chronic performance. Here, we review the state-of-the-art in electrode design, as well as the knowns and unknowns related to the biological response to key design features, to frame a discussion on the necessary next steps to formalize guiding principles for biologically-integrated electrode design.

2. Electrode design parameters: state-of-the-art

It is well documented that traditional metal- and silicon-based probes often elicit an undesirable immune response, typified by local neuronal loss and glial reactivity [26,27,38]. These observations have motivated the design of ‘next-generation’ devices which utilize sizes and materials that are smaller and more flexible than the standard approaches, and generally depart from more traditional designs in a variety of aspects, including unique architectures and insertion methods [39]. The novel approaches represented in next-generation devices seek, in part, to remedy the inconsistencies in the chronic performance of traditional probes. The current state-of-the-art encompasses a wide range of device attributes which are coupled to a relatively limited subset of biological assessments. Some of these next-generation devices have the potential to be commercialized and made accessible to the general public in the future. For ethical reasons, it is important that the biological impacts of new designs be better understood before next-generation devices are implanted long-term in human patients [40]. We have assimilated a description of design components of a variety of devices in table 1 and figure 1, and describe their features and reported effects on tissue response.

2.1. Metal based electrode arrays

2.1.1. Microwires

Microwires are traditionally fabricated from insulated stainless steel or tungsten wires, with

diameters typically ranging from 50–100 μm . As an early recording technology, detailed histological assessments of these devices were initially reported in the 1950s [41]. Collias and Manuelidis reported observations of marked hemorrhagic necrosis surrounding stainless steel microwires ($\sim 130 \mu\text{m}$ diameter) implanted in the cat brain at 24 h post-insertion, followed by neovascularization, microglial activation, demyelination, and astrocyte encapsulation in the following weeks. The tissue response became stable between the two- and six-month time points, and changes in glial and myelin appearance surrounding the device were generally unremarkable following the first month. A similarly stable chronic tissue-microwire interface was reported in the late 1990s, when Liu and McCreery described the response to EpoxyLite-insulated, 50 μm diameter platinum-iridium lead wires with iridium electrodes following implantation into the cat brain [42]. Based on the stability of the detected waveform shape, the authors reported that, ‘after implantation, the electrode-tissue interface may change from day-to-day over the first 1–2 weeks, week-to-week for 1–2 months, and become quite stable thereafter’ [42]. Post-mortem histology displayed minimal gliosis, thin fibrous encapsulation (~ 2 – $8 \mu\text{m}$ thick), and typically good proximity of electrode tips to local neurons (often within ~ 30 – $50 \mu\text{m}$ of the recording site). A more recent histological study of single stainless steel microwires insulated with EpoxyLite (75 μm diameter tapered to a 1 μm tip) implanted in rat cortex revealed persistent blood brain barrier leakage and inflammation throughout a twelve week time course [43]. Interestingly, neuronal loss and glial reactivity were relatively stable throughout the study, although the glial fibrillary acidic protein (GFAP)-positive region surrounding devices became more compacted and localized over time. This latter result deviates from the pronounced, progressive neuronal loss and glial encapsulation that are often observed surrounding silicon-based micromachined arrays.

2.1.2. Silicon-based shank arrays

‘Michigan’-style arrays (figure 1(A)) are micromachined planar devices with a tapered shape terminating in an apex with variable shank dimensions (commonly $\sim 120 \mu\text{m}$ maximum width \times ~ 15 – $50 \mu\text{m}$ thickness, with length determined based on the target structure of interest). These devices consist primarily of silicon with either iridium or platinum recording sites, where metal sites are deposited onto conductive traces (typically polysilicon, insulated with silicon dioxide and silicon nitride) embedded in the silicon shank [44, 45]. A key advantage of the technology is that the fabrication approach enables devices to be readily customizable into a wide variety of configurations (multi-shank, multi-modal, unique site configurations, etc). In an initial study which characterized the recording quality of these devices,

unit activity was detected with subject-dependent longevity up to a >4 month period [45], where over 90% of individual sites registered detectable unit activity. Nevertheless, results can be variable, and these electrodes are associated with an observable tissue response. A seminal study by Biran *et al* reported $\sim 40\%$ loss of neurons within the estimated recordable radius of the device and persistent microglial activation present over a four week implantation period [38, 46]. More recently, high-density silicon-based shank arrays have been developed by Masmanidis and colleagues, using newer fabrication techniques to achieve a minimum feature size of 0.4 μm (the minimum width of the conducting gold wires) [47]. The silicon shank had a geometry similar to more traditional ‘Michigan’-style arrays, with dimensions measuring $7\text{mm} \times 86 \mu\text{m} \times 23 \mu\text{m}$. The silicon shank supported 0.1 μm thick gold traces insulated by 0.5 μm thick layers of silicon nitride, and gold recording sites measuring $10 \mu\text{m} \times 10 \mu\text{m}$ in area. Individual shanks were separated by $\sim 300 \mu\text{m}$ patterned with 37 μm site spacing, allowing dense sampling of neural activity of various brain regions in mice (1024 sites implanted in total) [47]. While chronic recording performance and tissue response have yet to be fully characterized, and the biocompatibility of this device has yet to be characterized *in vivo*, the technology is promising for its ability to sample neuronal activity with high spatial resolution.

The Neuropixels probe (figure 1(C)) is another example of a high-density, silicon-based array and features >900 multiplexed channels on each individual shank [48]. The device physically resembles the Michigan array and has been developed to further improve the recording capabilities of current designs. The device is 70 μm wide by 20 μm thick with 960 titanium nitride (TiN) semiconductor recording sites located along the length of the array. Each TiN recording site is approximately $12 \mu\text{m} \times 12 \mu\text{m}$ with a thickness of 120 nm. The Neuropixels probe has significant recording advantages over the more traditional silicon-based Michigan array with respect to the unprecedented number of recording sites [49]. Preliminary data suggest that the recording capability of the device remains stable out to 60 d *in vivo*, and viable signals were obtained for 153 d in an exemplary animal [48]. Histological and other biocompatible metrics have yet to be utilized to evaluate the Neuropixels probe, so the precise measure of biocompatibility has yet to be determined.

2.1.3. Utah arrays

The Utah microelectrode array was developed by Normann and colleagues at the University of Utah (figure 1(B) [50–53]). The body of the device is doped (i.e. conductive) silicon, etched into 100 microneedles with SiO_2 insulating channels between them. They have an insulating layer of Parylene-C along most of the length. The base of each needle is approximately

Table 1. Overview of device design features and calculated bending stiffnesses. Bending stiffness was evaluated as previously described in [97].

Device	Components	Material	Dimension (width μm)	Thickness (nm)	Young's modulus (GPa)	Bending modulus (N M^{-1})	Reference
3D macroporous probe	Longitudinal interconnects	SU-8	7	800	2	6.64×10^8	Xie <i>et al</i> [72]
		Cr	5	1.5	140	9.48×10^8	
		Au	5	100	79	5.69×10^8	
	Transverse scrolling	SU-8	10	400	2	5.93×10^9	
		Cr	3	10–20, 1.5	140	2.37×10^8	
		Pd	3	80	16	3.56×10^2	
	Device bend arms	SU-8	6	800	2	2.37×10^2	
		Cr	4	1.5/30–50	140	2.44×10^3	
		Pd	4	80	16	3.06×10^3	
	Sensor metal contact	SU-8	5	800	2	5.00×10^2	
		Cr	4	1.5	140	6.88×10^1	
		Pd	4	50–80	16	1.85×10^1	
		Pt	4	100	168	1.48×10^7	
Syringe injectable probe	Polymer ribbons	SU-8	5–20 μm	350–400	2	2.37×10^5	Liu <i>et al</i> [73], Schuhmann <i>et al</i> [74,75], Zhou <i>et al</i> [76]
		Au	2–10 μm	100	79	9.28×10^1	
		Cr	2–10 μm	5	140		
Flexible parylene based multi electrode array	Planar shank (150 μm)	Parylene	150	20000	3.2		Xu <i>et al</i> [79, 80]
		Pt	45	200	168		
	Planar shank (100 μm)	Parylene	100	20000	3.2		
Polyimide	Planar shank	Pt	45	200	168		Chung <i>et al</i> [87], Dimensions: Tooker <i>et al</i> [85, 86]
		Polyimide	80	12000	2.5		
		Ti/Au/Pt	6	300	168		
		Polyimide	61	12000	2.5		
Carbon nanowire	Nanowire	Pt	6	300	168		Patel <i>et al</i> [92, 93]
		C	7	7000	234		
All diamond ultramicro-electrode	Polycrystalline diamond	(PCD) C	25	6000	1000		Rusinek <i>et al</i> [95]
		(BDD) C	19	3700	1000		
Michigan probe	Planar shank (thick)	Si	123	15000	179		Biran <i>et al</i> [38]
		Si	33	15000	179		
Nanoelectronic thread (NET-e-i)	Subcellular thread (min)	SU-8	8	800	2		Luan <i>et al</i> [100], Xiaoling <i>et al</i> [87]
		Au	0.2	16	79		
		Cr	0.2	4	140		
	Subcellular thread (max)	SU-8	8	1000	2		
		Au	0.2	200	79		
Cr	0.2	6	140				

(Continued)

Table 1. (Continued)

Device	Components	Material	Dimension (width μm)	Thickness (nm)	Young's modulus (GPa)	Bending modulus (N M^{-1})	Reference
Sewing machine thread electrode	Subcellular thread	Polyimide	16	4000	2.5		Hanson <i>et al</i> [89]
		Pt	4	130	168		
		SiO ₂	16	200	75		
NeuroPixels	Planar shank	Si	70	20000	179		Jun <i>et al</i> [48], Lopez <i>et al</i> [49]
		TiN	12	120	~200		

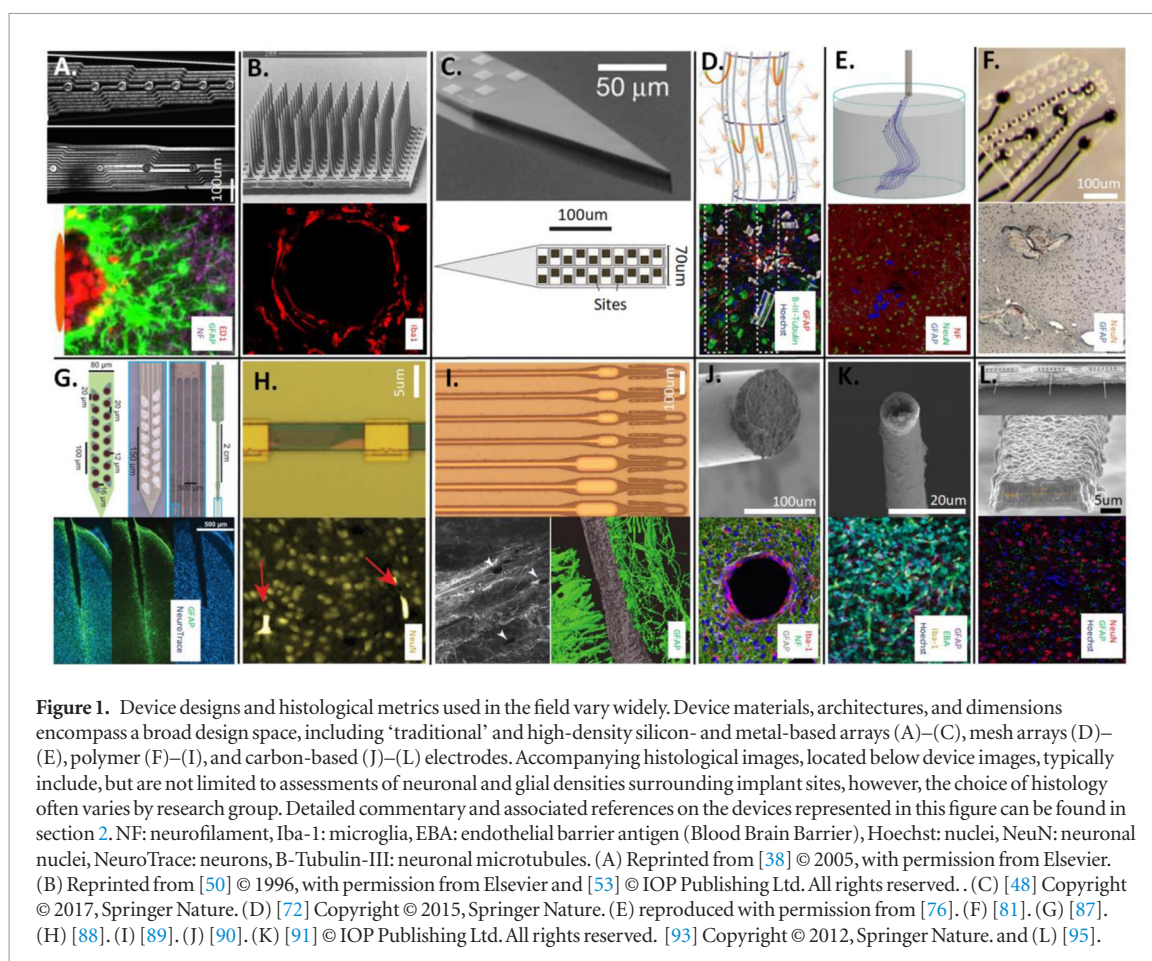


Figure 1. Device designs and histological metrics used in the field vary widely. Device materials, architectures, and dimensions encompass a broad design space, including ‘traditional’ and high-density silicon- and metal-based arrays (A)–(C), mesh arrays (D)–(E), polymer (F)–(I), and carbon-based (J)–(L) electrodes. Accompanying histological images, located below device images, typically include, but are not limited to assessments of neuronal and glial densities surrounding implant sites, however, the choice of histology often varies by research group. Detailed commentary and associated references on the devices represented in this figure can be found in section 2. NF: neurofilament, Iba-1: microglia, EBA: endothelial barrier antigen (Blood Brain Barrier), Hoechst: nuclei, NeuN: neuronal nuclei, NeuroTrace: neurons, B-Tubulin-III: neuronal microtubules. (A) Reprinted from [38] © 2005, with permission from Elsevier. (B) Reprinted from [50] © 1996, with permission from Elsevier and [53] © IOP Publishing Ltd. All rights reserved. (C) [48] Copyright © 2017, Springer Nature. (D) [72] Copyright © 2015, Springer Nature. (E) reproduced with permission from [76]. (F) [81]. (G) [87]. (H) [88]. (I) [89]. (J) [90]. (K) [91] © IOP Publishing Ltd. All rights reserved. [93] Copyright © 2012, Springer Nature. and (L) [95].

80 μm in diameter and a common geometry has needles 1–1.5 mm long at 400 μm pitch, though other geometries are possible. Tip metallization can be platinum or iridium based. The flat top of the device with a flexible wire bundle at a right angle to the needles enables it to ‘float’ with a brain that moves with respect to the skull, which made it well suited for use in primate brains [54, 55]. This device was brought under a quality management system throughout the early 2000s [56] for use in the Braingate clinical trial [57]. It has since become the most widespread implant used in humans. A recent literature search reveals 48 human implants as of 2018 [58], primarily in epilepsy or intraoperative studies, with 18 chronic implants done for a mean number of 578 d under an investigational device exemption (e.g. [17–19, 59–61]).

However, due to predominant use in large animals and humans, very little is known about the long-term immune response of these devices. Early studies in cat visual cortex suggested that scarring was limited to $<10 \mu\text{m}$ from the electrode [51, 62]. Also, both human and monkey experiments are typically conducted across years, long after the 6–8 week period of scar formation, sometimes for as many as 5–7 [63–65]. This suggests that at least a subset of neurons survive the scarring process. However, based on rodent studies [66–68], we know that the scarring, and even long term remodelling may be substantial [53]. This has likely been limiting the neuronal yield of these devices from the beginning. Gradual degradation after 8 weeks may be dominated by materials failures [69, 70] due to a warm, salty environment across many years [71].

2.2. Polymer and next generation electrode arrays

2.2.1. 3D macroporous probe

A common goal in the design of ‘next-generation’ devices is to employ flexible substrates with small feature sizes to close the gap in the mechanical mismatch between devices and host tissue. The three-dimensional (3D) Macroporous Probe developed by Charles Lieber’s group is a two-dimensional mesh that has been folded into a semi-cylindrical shape with a blunted end. This device has a greater structural complexity when compared to standard shank devices. The bulk of these devices is composed of an insulating SU-8 photoresist layer. For added structural integrity and flexibility, multiple aspects of this design also include palladium and chromium within non-recording, global ‘scrolling’ elements. This electrode is complex, and consists of multiple components including the ‘longitudinal interconnects’, ‘transverse scrolling’ elements, ‘device bend arms’, and the sensor contacts (see figure 1(D)). The longitudinal interconnects of the device comprise the majority of the device. The longitudinal component consists of an 800nm thick by 7 μm wide ribbon of SU-8 photoresist with a 100 nm gold metal trace with a width of 5 μm . The transverse element is a ribbon of SU-8 photoresist of the same thickness but a greater width (10 μm). The transverse element maintains the structure and flexibility of the device and contains a palladium/chromium core with a thickness of 80nm and width of 3 μm . The device bend arms house the recording elements (100 nm thick platinum sites which are 4 μm wide), which extend outward from the main structure following implantation. The bend arms provide the unique feature of allowing the recording elements to drift away from the body of the device, potentially escaping downstream immune response. Insertion of this device was facilitated by flash-freezing in liquid nitrogen to temporarily maintain structural stability during implantation.

Following implantation, the macroporous probe shows an initial void of tissue following injury at acute timepoints. This void appears to regenerate after five weeks with a sustained, but modest level of gliosis surrounding the device. Histological analysis suggests that neuronal cell bodies and glia are present in close proximity to the device both within and outside the structure of the mesh. The results presented by this device design appear to be markedly better than traditional planar device architectures [39, 72].

2.2.2. Syringe injectable probe

In addition to the macroporous probe, syringe-injectable electronics have been developed by Lieber’s group (figure 1(E)). Much like the 3D macroporous probe, the syringe injectable probe is a 2D mesh made from planar ribbons of polymer and metal with incorporated recording elements. The bulk material of the syringe injectable mesh is SU-8 photoresist with internal metal components that include trace

chromium, gold interconnects, and platinum recording sites. The SU-8 ribbon has a total thickness of 800nm and ranges from 5 μm to 20 μm wide. The metal traces of chromium and gold have a cumulative thickness of 105nm and a width that ranges from 2-10 μm [39, 73–76]. Histological evaluation shows that the syringe injectable mesh has improved biocompatibility in comparison to planar polymer thin-film probes. Over a three-month time period, the injectable mesh has a smaller footprint than planar polymers. Syringe injection of the electrode mesh has a noticeable footprint at the 2-week time-point that is represented by loss of neuronal nuclei, disruption of neuronal processes, and an increase in proximal astrocytes. However, the footprint of the mesh is relatively much smaller than the polymer thin-film that was used as a comparison. The improved tissue integration becomes more apparent at the four-week and three-month timepoints. The planar polymer control exhibits a stereotypical chronic immune response with an increased loss of neuronal cell types and a much larger accumulation of astrocytic scar tissue by the three-month time-point. The mesh probe, however, at four-weeks and beyond shows a regeneration of neuronal processes into and around the electronic mesh and a disappearance of GFAP positive cells. The four-week timepoint suggests that neuronal density is still diminished near the device, but histology at the three-month time-point shows that neuronal cell bodies are present proximally and within the structure of the mesh [39]. This concept of creating finely featured devices that mimic the structure of neuronal morphology has also been expanded on in the form of the ‘neuron-like electronics’ (NeuE) probe [77].

In a unique approach, Trevathan *et al* have developed a new strategy for an ‘injectable electrode’ [78]. This novel electrode uses an uncured solution containing conductive elements which polymerizes into a functional neural interface following injection into the body. The cured polymer interface is highly compliant and can encapsulate target nerves. These devices were evaluated using a battery of tests to characterize the electrical and mechanical performance characteristics. Sufficiently percolated material with a silver content level of at least 65% w/v was found to have an impedance of less than 10 M Ω , whereas ‘injectrodes’ with silver content below 65% maintain much higher impedances. The estimated Young’s modulus of a cured injectable electrode is 65 kPa, which is orders of magnitude lower than traditional electrode materials such as silicon. Injection of this device could theoretically be altered to form specifically sized features to enhance biocompatibility. Histological results are limited and no observations have been reported to-date outside of the peripheral nervous system. Additional characterization is needed to fully assess the biocompatibility of this device, particularly for future applications in the brain.

2.2.3. Flexible Parylene-C

Ellis Meng's research group has reported a flexible Parylene-based array (figure 1(F)) to chronically record from the rat hippocampus. The recording sites of the hippocampal array are precisely laid out to match the unique shape of hippocampal projections. This array consists of tapered planar shanks with embedded platinum traces and recording sites. The proximal area of the Parylene probe is approximately 20 μm thick and 150 μm wide. The 150 μm shank tapers down to an approximate 100 μm width. The platinum recording sites are 200 nm thick and approximately 45 μm wide. The changes in bending stiffness (the measured material resistance towards deformation) along the taper are considered to be negligible [79]. Parylene devices successfully recorded single unit activity throughout the entirety of a one-month period, and some observations suggest that Parylene devices can remain viable *in vivo* out to one year. While the chronic histological evaluation of these devices has yet to be fully characterized, Parylene-C has been designated as a class VI United States Pharmacopeia biocompatible material [79, 80]. Histological analysis was performed on implanted brains at time points up to one-month post implantation. Initial histological results and cresyl violet stains suggest that properly implanted Parylene devices display minimal tissue reactivity aside from a suspected microglia sheath at one-week post implantation.

Meng's group has also developed a Parylene sheath electrode that can be implanted with the aid of an assistive microwire. This device is approximately 7-10 μm thick with a width that tapers from 300 μm to 50 μm . Each sheath contains 8 platinum electrodes with a 45 μm diameter. The sheath structure also contains perforations that allow tissue to invade the structure of the device and to facilitate cellular signalling across the Parylene structure. This device can be coated with a variety of bioactive components such as Matrigel to potentially further enhance biocompatibility. This electrode has been reported to detect activity *in vivo* for up to 50 weeks [81].

Histological evaluations from alternate Parylene-based devices have shown generally good tissue integration and biocompatibility. Seymour and Kipke published a seminal report which explored the impact of feature size on tissue response using a Parylene-coated, 'Michigan'-style device using an SU-8 backbone [82]. Here, electrodes are displaced from the main shank using support arms with varying dimensions; importantly, neuronal loss and gliosis were mitigated surrounding the subcellular features of the device. Purcell and Seymour explored the idea of a hollowed-out, planar, Parylene-coated probe designed to incorporate a neural stem cell-seeded scaffold [83]. The two main arms of the device are bulk SU-8 with a 5 μm thick Parylene-C coating on each face. The total of the support arms are 42 μm thick and 45 μm wide. The hollow structure that houses the alginate scaffold has

a 110 μm width and variable thickness. When seeded with stem cells, the devices resulted in an initially decreased acute immune response and an increase in neuronal densities following implantation. The mode of influence may be a 'bystander' effect (providing trophic support) rather than direct differentiation and integration into surrounding tissue [84]. However, these effects were transient, and the increase in neuronal density declines beyond six-weeks, at which point neuronal densities more closely match control conditions and glial encapsulation becomes present around all devices.

2.2.4. Flexible polyimide

Intracortical polyimide-based devices were described roughly two decades ago by Rousche and colleagues, who initially reported successful, short-term recording capabilities of devices fabricated with standard photolithographic techniques [85]. Characterization of the devices was relatively limited, but a variety of architectures were presented, including devices presenting embedded wells for delivery of bioactive substances. Recently, the flexible polyimide probe designed by Loren Frank's group has advanced the use of polyimide based-devices as previously described (figure 1(G)) [84-86], demonstrating efficacy in recording unit activity over a ~5 month time frame. The device is a 16 channel planar shank device with a total width and thickness of 80 μm and 14 μm , respectively. The bulk material used in this approach is polyimide with a total thickness of 12 μm and a width of 80 μm . The trace metals used consist of titanium on gold with either platinum or iridium recording sites. The trace metals share a thickness of approximately 300 nm at 6 μm wide. Additionally, polyimide is a compatible material surface for the utilization of bioactive surface modification [86]. The polyimide device was capable of recording single units over a period of 283 d post-implantation, albeit with a decline over time. This device has yet to be fully characterized by histology *in vivo*, but available coronal histology shows an apparent lack of astrocyte encapsulation of the device after 160 d post-implantation. The extent of the glial encapsulation has yet to be directly compared to standard technologies [86].

2.2.5. SU-8 nanoelectronic thread electrodes

The Xie lab has created an SU-8 based electrode by utilizing both photolithography and electron beam lithography (EBL) (figure 1(H)). These 'nanoelectronic thread' (NET) electrodes can be fabricated with dimensions as small as 0.8 μm \times 8 μm [88]. This device is also inserted with the aid of a shuttle device that interacts with the implanted electrode in a similar way that a sewing needle interacts with thread. The shuttle device is made from a <10 μm diameter carbon fiber with a smaller 3 μm diameter tip that has a length of 4 μm . The shuttle device engages with a micro-hole at the apex of the NET electrode and disengages

from the electrode as the shuttle is retracted after the target depth is reached. This device was inspired in an effort to expand on the capabilities of devices such as the Utah array. The NET electrode consists of two insulating 300–500 nm layers of SU-8 fabricated with photolithography, as well as EBL-defined 100 nm gold interconnects and a 2–3 nm chromium adhesion layer. Histological evaluations were performed at two- and four-months post-implantation. 3D reconstruction of vasculature surrounding implanted NET electrodes suggest that there is no significant leakage of capillary networks at chronic timepoints. Other histological evaluations of neuronal morphology show that the subcellular NET electrodes can form tight interfaces with neuronal populations without any apparent disruptions to neuronal morphology. At four months post-implantation, any reduction in neuronal cell density is likely recovered as observed by neuronal nuclei stains. Insertional trauma has yet to be reported, but chronic histology does suggest that damage to the tissues surrounding implanted devices recovers in a promising way. Histological evaluation of gliosis has yet to be reported using these devices.

2.2.6. 'Sewing machine' polymer probe

This approach uses small thread electrodes made from polyimide (figure 1(I)), similar to the NET probe, and utilizes an automated insertional shuttle in the form of a 'sewing machine' style device [89]. The robotic sewing machine device is designed with the goal to reliably implant devices with minimal vasculature damage through the aid of an Erythrosin-B saline stain of the dura. The ability of these devices to be robotically implanted with high levels of fidelity is highly attractive in biomedical and research applications. The device is fabricated from two separate layers of $2\ \mu\text{m} \times 16\ \mu\text{m}$ polyimide, platinum or gold traces $130\ \text{nm} \times 4\ \mu\text{m}$, 400 nm copper, 5–6 μm Parylene, and a hard mask of 200 nm silicon dioxide on the basal side of the electrode. The total width of the shank is $16\ \mu\text{m}$ with a total thickness of approximately $10\ \mu\text{m}$. Preliminary histology conducted on slices surrounding these devices suggest that astrogliosis is also present near the implanted sewing machine devices. However, detailed analysis of biocompatibility at chronic timepoints has yet to be reported using the devices.

2.2.7. Polymer microwire

Tracy Cui's ultra-soft polymer wire electrode (figure 1(J)) is a combination of poly(fumaric acid-co-1,7-octadiene diepoxide-co-terephthalic acid) polyethylene glycol (PFOT-PEG) and polydimethylsiloxane (PDMS). The ultra-soft microwire was designed largely due to the historical mechanical mismatch between neural tissues and traditional devices. The ultra-soft microwire electrode array has a diameter of $125\ \mu\text{m}$ and is fabricated via extrusion of poly(3,4-ethylenedioxythiophene) polyethylene glycol (PEDOT-PEG) conducting

polymer and PDMS through a 29-gauge syringe needle. The resulting Young's modulus for these soft microwires is 974 kPa. Following extrusion, electrodes are coated in fluorosilicone. The device was implanted via a stainless steel shuttle and evaluated in the brain for either 1 or 8 weeks [90]. Results were compared to relatively stiff tungsten devices of identical size and shape. The soft electrodes facilitated neuronal adherence to the outer surface without any apparent deleterious effects. *In situ* imaging of sectioned microwire electrodes showed that neurons surrounding the device underwent significantly less deformation when compared to stiff metal electrodes. Over the course of 8 weeks, tissue surrounding the microwire electrodes displayed fewer microglia and macrophages (Iba-1), reactive astrocytes (GFAP), and less evidence of cleaved caspase-3 (a marker of neuronal apoptosis) or distortion of mature axons (NF200). Blood brain barrier (BBB) leakage also was reduced around the soft electrodes compared to stiff electrodes. Devices were explanted at each timepoint and histologically stained to characterize cellular adhesion to the device. In general, soft devices showed a greater level of adherent cells after explant compared to stiff devices. Of the cell types analyzed, beta-tubulin positive neural cells appear to make up the bulk of adherent cells [90].

2.2.8. Carbon microthread electrode (MTE)

In 2012, Kozai and colleagues reported the chronic recording performance of a novel, carbon fiber-based recording electrode with subcellular dimensions [91]. The device was an ultra-small $7\ \mu\text{m}$ diameter carbon fiber with a conductive poly(3,4-ethylenedioxythiophene) (PEDOT) coating at the distal end for recording and an insulating bulk coating of 800 nm poly(p-xylylene) and 50 nm poly((p-xylylene-4-methyl-2-bromoisobutyrate)-co-(p-xylylene)). While carbon has a Young's modulus of $\sim 200\ \text{GPa}$, it has a competitive composite bending stiffness at a $7\ \mu\text{m}$ diameter (table 1). As such, this microelectrode is relatively flexible, but it can be implanted into the cortex with the aid of an assistive insertion device [91]. Chronically implanted MTEs show a markedly improved tissue response compared to implanted silicon-based 'Michigan' probes, with greater interfacial neuronal densities and lower accumulation of proximal astrocytes, microglia, and endothelial cells. Such improvements in biocompatibility may be due, in part, to the relatively small footprint of this device. The MTE is one of the smallest freestanding implantable devices, and therefore, it is able to 'stealthily' interface with the brain by minimizing BBB disruption and tissue displacement. In addition to being relatively biocompatible, MTEs have been shown to provide stable recordings out to 5 weeks *in vivo* and are also capable of single unit recordings [91].

More recently, Paras Patel and Cynthia Chestek have further developed this technology through the testing of different tip coatings (figure 1(K)), fabricating MTEs into an array configuration, and evaluating the array *in vivo*. First, MTEs were coated in poly(3,4-ethylenedioxythiophene):p-toluene sulfonate (PEDOT:pTS) as opposed to poly(3,4-ethylenedioxythiophene)-poly(styrenesulfonate) (PEDOT:PSS) and were aged at an accelerated rate in a heated bath. Overall, the PEDOT:pTS devices were found to have more extended longevity than the PEDOT:PSS probes and were selected for chronic *in vivo* characterization [92]. The new arrays consisted of 16 MTEs in a 2×8 configuration with a pitch of $152.4 \mu\text{m}$. Insertion of the arrays was accomplished with a sacrificial layer of polyethylene glycol (PEG) that encapsulated the MTEs during insertion, but was dissolved just as the fibers penetrated the brain [93]. Chronic implantation of the arrays showed similar neuronal survivability around the device interface and reduced foreign body response as seen in Kozai *et al* [94]. While the devices maintained recording fidelity out to 112 d [93], there is still a disconnect between the nearly non-existent immune response and the overall recording yield/longevity. These results indicate that while mitigating tissue response plays an important role in long-term recording yield, other factors such as tip coating preparation and the stability/degradation thereof, may also be critical to chronic electrode performance.

2.2.9. Diamond ultramicroelectrode

Diamond is an emergent electrode material owing to its biocompatibility and suitability for both electrophysiological and neurochemical measurements. On the latter point, the wide potential window, low capacitance, and low background current of conductive, boron-doped polycrystalline diamond (BDD) are attractive features for fast scan cyclic voltammetry for neurotransmitter detection [95]. Li and colleagues have fabricated an all-diamond electrode array featuring a BDD core that is insulated by a thin layer of polycrystalline diamond (PCD) (figure 1(L)). The internal BDD core is $3.7 \mu\text{m}$ in thickness and $19 \mu\text{m}$ wide, and including PCD insulation, shank dimensions are approximately $6 \mu\text{m}$ thick by $25 \mu\text{m}$ wide (although, devices can be fabricated in a range of feature sizes). PCD is a mechanically robust material with a Young's modulus of approximately 1000 GPa. Despite the exceptionally high Young's modulus, the ability to fabricate devices with subcellular dimensions ($<10 \mu\text{m}$) allows for these devices to maintain a reasonable bending stiffness [95]. Histological characterization of these devices *in vivo* is ongoing.

3. The relationship between electrode features and biocompatibility

Assimilating the impacts of electrode features on biointegration is challenging due to the wide

assortment of next-generation electrodes under development and the lack of standardized testing regimens across laboratories. Here, we review reported observations linking electrode features to histological outcomes and describe strategies to modify probes to improve tissue integration.

3.1. Stiffness and feature size

Studies suggest that the architecture and flexibility of devices play important roles in determining effective tissue integration: device cross-sectional dimensions, Young's modulus, and bending stiffness have all been identified as key features of design. An early study by Szarowski *et al* indicated that initial insertion damage and reactivity within the first week of implantation is proportional to the cross-sectional area of the device, but that responses were insensitive to device geometry in the chronic assessment period (>4 weeks) [96]. The authors concluded that they had observed, 'an early response that is proportional to device size and a sustained response that is independent of device size, geometry, and surface roughness'. However, in support of the importance of device dimensions in determining tissue response, later studies revealed that gliosis and neuronal loss were mitigated when device features were reduced to a subcellular scale ($\sim 5 \mu\text{m}$ thickness) [82]. Likewise, $7 \mu\text{m}$ diameter insulated carbon fibers with PEDOT-functionalized electrode tips display a negligible tissue response, which may be attributable to their minimal footprint [91]. In combination, these observations suggest that electrodes with subcellular dimensions ($\lesssim 10 \mu\text{m}$) result in improved tissue response. Reduced Young's modulus has also been credited with improved tissue integration, based on studies that have examined the response of BBB leakage, as well as microglia/macrophage, astrocyte, and neuronal densities proximal to various planar probes of differing stiffnesses. In experiments in which devices ranging from 6 MPa to 150 GPa were evaluated, the foreign body response appeared to plateau at stiffnesses of 1.5 GPa and below [97]. Nevertheless, a recent meta-analysis indicated that it was not feature size or Young's modulus that most strongly determined the degree of tissue response, but rather bending stiffness [98], which incorporates feature dimensions, 'softness'/Young's modulus, and cross-sectional shape into its calculation. In summary, combining observations across these initial studies indicates that smaller, softer devices favor improved tissue integration. However, studies which directly assess the impact of device features on biocompatibility are relatively scarce and disparate in methodology, and questions remain regarding the generalizability of observations and underlying mechanisms.

For instance, the primary motivator for the movement toward softer, more flexible electrodes is to remove the mismatch in mechanical properties between brain tissue and devices, thus creating a more

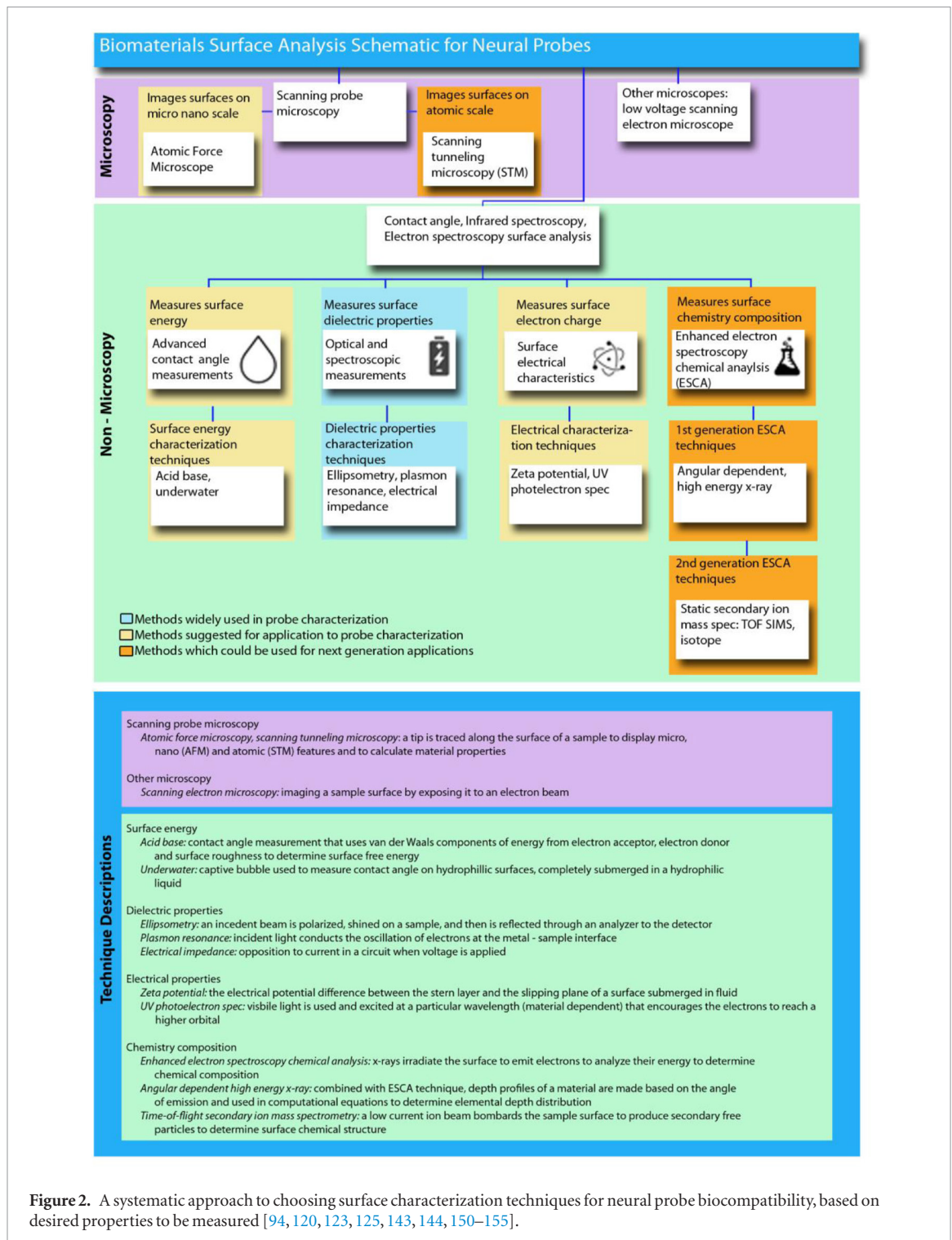
seamless interface. However, a first question pertains to what, exactly, are the mechanical properties of brain tissue? Since it is difficult to quantify the mechanical properties of human brain tissue *in vivo* and *in situ*, literature characterizing brain tissue mechanical properties are widely varying. A myriad of tissue preparation methods [99–102], temperature [103–105], post-mortem times [102, 105, 106], and testing such as rheometry [107–109], magnetic resonance elastography (MRE) [107, 108, 110], shear wave elastography [111], and atomic force microscopy (AFM) [106, 109, 111], are used, resulting in a range of values, 35–422 100 000 Pa [112], that vary by eight orders of magnitude (summarized in supplementary table 1 (stacks.iop.org/JNE/17/021001/mmedia)). Many characterization studies occur not in the human brain, but in animal models such as rats and mice, which further complicates this view since murine models have fewer striations, surface area, different pharmacokinetic profiles, and distinct structural organization in comparison to human brains [113, 114]. These uncertainties make it challenging to accurately predict the desired elastic modulus to minimize micromotion at the implantation site and adequately ‘match’ the properties of brain tissue. Furthermore, neurosurgeons have reported regional variation in stiffness in the brain [115], which suggests that, depending on the function of the probe and the area in which it is implanted, that each probe may require a different design.

Nevertheless, polymer, hydrogel, and nanocomposite-based materials have been introduced as possible solutions to create softer devices and facilitate tissue integration [116]. The use of Parylene-C and polyimide is primarily motivated by the improvement in Young’s modulus in comparison to metal- and silicon-based electrodes (table 1). Likewise, hydrogel coatings have been implemented to create a softer, more tissue-friendly interface [117]. Newer approaches utilize materials that are initially rigid (facilitating insertion), but transition to more compliant materials following contact with the *in vivo* environment. Hybrids and composites, such as nanocomposites based off of the architecture and structure of sea cucumber dermis [118], allow for mechanical tuning *in vivo* [119]. Polyvinyl acetate structures enable changes in electrode compliancy to minimize the foreign body response [118, 120] via this mechanism. The biomimetic nanocomposite is comprised of a low modulus polymer and cellulose-based nanowiskers that swell when hydrated or inserted in the brain, resulting in a decreased modulus due to increased water content by volume, on a timescale of 5 min. The tissue response was characterized by a 50 μm neuronal ‘kill zone’ and a decrease in glial reactivity [121, 122]. Similarly, thio-ene/acrylate substrates, polymerized via click chemistry reactions on the surface of the probe decrease shear modulus from 460 MPa to 2.3 MPa. Softening of the substrate upon hydration, a week after implantation, facilitates neural function

[123]. Substrates were an order of magnitude stiffer than tissue, but the modulus mismatch was reduced in comparison to stiffer substrates. Bioresorbable interfaces, termed ‘live electrodes’, improve acute and short term foreign body response by utilizing biocompatible mesh/microporous structures that integrate with environment, minimize electrode-neuron distance, and support the mechanical and biochemical environment of the neurons [116]. Other biologically active compounds such as silk [124] and the fibroin derived enzyme, chondroitinase (chABC) [125], have been used to address the issue of mechanical mismatch by using the enzyme to dissolve the chondroitin layers of the scar tissue that encapsulates the probe.

3.2. Device tethering

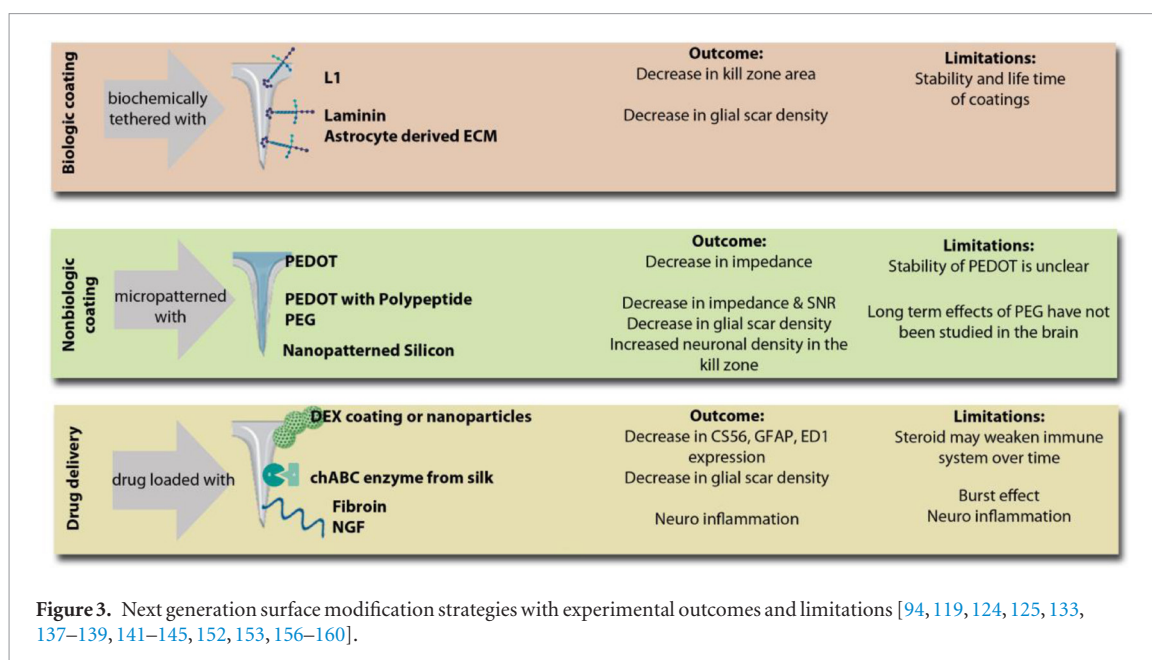
Tethering forces exerted by the connector configuration can also influence the tissue response. Traditional devices are generally either free-floating in the brain tissue (untethered), mounted to a connector fixed to skull-mounted bone screws (skull-fixed), or semi-floating (e.g. flexibly tethered to a connector via a ribbon cable encased in elastomer). Skull-fixed devices lack the ability to compensate for natural micromotion and swelling of the brain, which may lead to increased irritation and damage in interfacial tissue. In 2005, the mechanical effects of implanted CNS electrodes on surrounding tissue were investigated using finite element modelling. Device analogues for silicon, polyimide, and a hypothetical ‘soft’ material were evaluated *in silico*, and simulation results suggested that devices made from stiffer materials exacerbate shear strain along the device-tissue interface. Shear strain from skull-fixed devices can impact tissues out to 100 μm from the interface and result in delamination of tissue from the device. In turn, these effects may further aggravate the chronic immune response associated with implanted electrodes. The model produced in this paper suggested that interfacial strain on host tissue could be mitigated by 65%–94% by adopting more flexible materials such as polyimide [126]. These results were corroborated by *in vivo* results collected by different groups during evaluations of free floating and tethered cortical silicon devices [127, 128]. Histology showed that, in comparison to untethered counterparts, tethered devices elicit greater levels of immune response at the tissue interface. The depletion of local neurons, increase in GFAP positive astrocytes, and upregulation of ED1 positive microglia and macrophages were all notably worse surrounding tethered devices. Next-generation devices often adopt materials and architectures that may better accommodate micromotion and mitigate device-tissue strain, offsetting the relative impact of tethering on the tissue response. Nonetheless, it is still essential to consider device fixation as an additional design variable that can significantly impact the biocompatibility of implanted electrodes.



3.3. Surface features and modification strategies

Surface chemistry and topographical cues have received relatively lesser attention from the device design community than architecture and flexibility/softness; nonetheless, their impacts are inextricably intertwined with the incorporation of new materials in next-generation designs (figure 1). The surface variables that can be measured and controlled are: hydrophilicity, chemistry, and surface topography. Contact angle/wettability measures surface energy, spectroscopy determines chemical composition, and scanning probe technique characterizes

micro-level topography (figure 2). While there are no field-standard guidelines, contact angles measured ideally should be low, indicating high surface energy in the range of 40–80 dynes cm^{-1} . This is the range at which materials are hydrophilic enough to favor hydrogen bonding between the biomaterial surface and surrounding fluid over the hydrophobic interactions which favor protein adsorption [129]. Foundational studies have reported the fundamental physical characteristics of the surfaces presented by materials commonly used in electrode design. Polyimide is a hydrophobic material (contact angle reported between



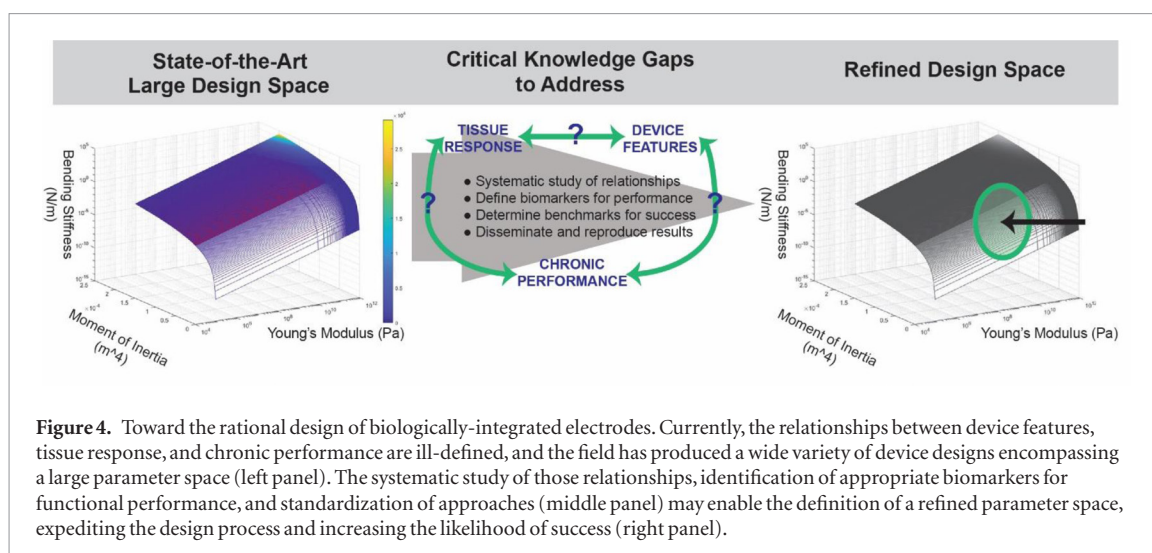
80–100°) with an associated high adsorption of proteins [130]. Nonetheless, it exhibits low cytotoxicity and hemolysis, in alignment with biocompatible materials that served as a benchmark in the study (Teflon® and Silastic®). Parylene-C is similarly hydrophobic and biocompatible, although plasma treatment can be used to render the surface hydrophilic [131]. Silicon has been shown to be comparatively less biocompatible (in terms of thrombogenicity) than its polymeric counterparts, Parylene and polyurethane [132]. SU-8, while generally regarded as a highly biocompatible polymer, reportedly displays similar hemocompatibility to silicon, with similar platelet reactivity and thrombogenicity [132].

Specific surface cues have been observed to be especially amenable to neuronal growth and responsiveness [133–135], and the dimensions of topographical features are known to influence effects: optimal promotion of neuronal growth occurs when the spatial pattern for controlled directionality matches the dimensions of neuronal growth cones [136]. Preliminary reports from Erefej and colleagues in the Capadona lab suggest that nuanced topographical and architectural changes can impact the expression of pro-inflammatory factors surrounding neural implants. In an experiment where traditional planar probes were etched to form small, 200 nm high grooves across the length of the probe, tumor necrosis factor alpha (TNF α), nitric oxide synthase (NOS2), and a chromatin protein, high mobility group box 1 (HMGB1), were upregulated in the un-etched devices. The patterned probes showed a downregulation of the lipopolysaccharide binding receptor CD14 expression over a 2–4-week time-period which may suggest a trend towards increased regeneration as microglia and monocyte populations return to baseline. These results suggest that smooth planar shanks may create a more continuous expression of interleukin 1 beta (IL1B), resulting

in prolonged BBB leakage, and potentially upregulated TNF α and NOS2 as a downstream consequence [137].

Given the rationale for surface-mediated control of biocompatibility, numerous strategies have emerged in the field to influence biocompatibility through modifications to implanted electrode surface features (figure 3). Biomimicry—making the device invisible to brain tissue by imitating its key features—is one strategy to address device failure and improve long term function and ‘mask’ the device from its surroundings. Biologically active materials such as L1 (neural adhesion molecule) have been coated on Parylene-C microwires and shown to decrease markers of apoptosis and astrogliosis at the injury site [138] and improve neuronal growth and survival around the implant [139]. Alpha melanocyte stimulating hormone (Alpha-MSH) [140] has also been proven to lower expression of markers of gliosis while chABC delivery likewise has been reported to reduce ionized calcium binding adaptor molecule (IBA1) and chondroitin sulfate (CS) expression [141]. Recently, Oakes *et al* used a decellularized bovine astrocyte derived extracellular matrix (ECM), traditionally used in emergency rooms to promote wound healing, to coat Michigan-style arrays. The coating reduced the amount of astrogliosis, hemostatic activity, and macrophage activation *in vitro* [142]. However, the short life time of the coating limits an effective response to chronic or long-term foreign body response.

Drug-eluting or drug-presenting surfaces are another avenue to modulate device-tissue integration. Dexamethasone (DEX) coated [141] and DEX loaded probes [143] have been shown to decrease anti-chondroitin sulfate antibody (CS56), GFAP, and ED1 expression in surrounding tissue as well as reduce impedance by up to 25% for 9 d. However, there are also limitations surrounding long term tethering of biologically active molecules on these probes with



reports of cracks in DEX film coatings at four weeks [144], and observations of the ‘burst effect’ [145]. Future improvements may include prolonged drug release, better drug adherence to the surface, and increased drug loading/release for enhanced efficacy [144].

4. Outlook: perspective on critical knowledge gaps in the field

While many of these approaches to improve tissue compatibility have delivered evidence of positive results, they also have saturated the field with a multitude of designs that change multiple variables simultaneously. Furthermore, foundational understanding of benchmarks for success, clear goals for longevity and integration, and standardization of approaches across users are lacking in the field. Here, we make recommendations for studies to be pursued to reconcile current barriers to progress to achieve a seamless, chronic electrode interface (figure 4):

- (1) A systematic study of the relationship between device design features (materials, architecture, flexibility), biointegration, and signal quality needs to be performed, and interaction effects between different features of design need to be parsed apart to reduce confounds in data interpretation.
- (2) Benchmarks for success need to be determined (biological integration, recording performance, longevity, stability).

As reviewed above, several design aspects may influence the biocompatibility and signal detection of implanted electrode arrays in the brain. However, studies which explore these effects in a systematic way are scarce, and it is extremely challenging to truly parse apart individual effects. For instance, the effects of Young’s modulus on tissue response may require the use of multiple material types to produce the desired range of flexibilities (e.g. silicon, polyimide, and off-stoichiometry thiol-ene-epoxy (OSTE+) polymer) [97]. While it is possible that the effects of surface chemistry could be negligible, there remains

the potential for differences in topology, hydrophobicity, and cytotoxicity to affect results (figures 2 and 3). Furthermore, the surface charge, topography, size and geometry could all synergistically affect biocompatibility of the device as a whole. A study published by Capadona and colleagues effectively decouples the impact of surface chemistry and substrate stiffness (in terms of Young’s modulus) on the biocompatibility of implanted electrodes by coating all substrates with the identical polymer [146]. Nevertheless, bending stiffness and geometry remain important considerations to integrate into such analyses. If such effects could be studied in a more broadly systematic way, the value and interpretation of the data collected from these, and other studies, would be greatly enhanced. A central challenge is that the parameter space would be expansive, requiring a large sample size and an extensive observation set for each sample. However, prioritizing testing of selected high-value features of the greatest relevance for current designs could make this seemingly intractable study achievable.

What makes a ‘good’ chronic electrode? In terms of biocompatibility, what tests are the most relevant for predicting safety and performance? According to ISO 10993-1, because electrodes are permanent implant devices with external communication capabilities that come in contact with blood and brain tissue, probes should be subjected to cytotoxicity, sensitization, irritation, acute and subchronic toxicity, implantation, hemocompatibility, and carcinogenicity testing (ISO 10993) (Supplementary Table 2). However, relatively limited controlled biocompatibility testing occurs in pre-clinical reports, and read-outs heavily depend on metrics of neuronal and glial densities. Based on these metrics, it has been suggested that critical ‘thresholds’ of device flexibility and feature

size can be identified for optimal device-tissue integration [82, 96]. Likewise, a recent meta-analysis suggests that bending stiffness is the strongest design-related predictor of neuronal and glial responses [98]. However, available observations suggest that there is not a simple relationship between the traditional metrics of tissue response and chronic function [147], underscoring the need to better understand which aspects of the biological response to electrodes most profoundly and predictably affect their function. If those markers of the tissue response were identified, it may simplify and standardize assessment of the biological response to electrodes. For instance, are changes in cellular densities (neuronal and glial) most strongly predictive of device function, or are particular markers related to certain functional signalling pathways, or sub-cellular structural remodelling (as a few possibilities) the most important? While assessments of new electrode design almost invariably test their impact on local neuronal and glial densities, these metrics have not been validated as effective benchmarks for success in terms of recording quality: it may be the case that some other aspect of the biological response is more directly deterministic of functional outcomes.

Recent evidence suggests that chronic implantation of neural interfaces results in changes in intrinsic neuronal excitability at the protein level [28, 29]. The proteins that have been currently explored outside of cell type specific markers are ion channels and transporters that may influence cellular excitability. These data suggest that there may be effective biomarkers for biocompatibility of implanted devices that investigate mechanisms beyond cellular density. In order to drive the field forward in a more constructive way, it is imperative that future research includes a more thorough evaluation of biocompatibility at the cellular and molecular level. This would ideally include traditional histological analyses as well as acute and chronic genetic changes at the transcriptional level [137]. In doing so, there is a possibility to define biocompatibility at a deeper level that results in identifying key bio-integrative electrode features and potential targets for intervention following implantation.

- (3) User results and methods, particularly those that champion a specific design or electrode modification, need to be replicated across laboratories.

A related challenge is centered on the approach needed to unmask ‘master’ biological signalling pathways that influence performance: there is a need to identify more effective and reproducible testbeds to refine electrode design and benchmark results between technologies. Correlation between device functional metrics and histological outcomes may be a reasonable point of departure to assess device-tissue integration within individual labs, but ultimately, direct methods to determine the most relevant mechanisms with

improved specificity and control will be required. Likewise, given the expansive set of potential pathways at play, the identification of the most important changes in protein or gene expression amongst the many available possibilities is a major challenge. Developing a high-throughput testbed to assess the impacts of design features on tissue response would be extremely valuable to the field. Likewise, incorporating broad-based assessment strategies which avoid pre-selecting targets of interest could reveal that the expression of unexpected targets which bear a stronger relationship with recording quality than previously-studied metrics. Accounting for inter-areal and inter-species differences will be important in these analyses, given the potential for brain microenvironment heterogeneity to influence results. Likewise, insertion methods vary between users, and the relationship between chronic histology and the initial surgical approach should be studied. As an example, the presence of reactive astrogliosis surrounding ‘sewing machine devices’ is notable, since the electrodes are designed with subcellular dimensions and are fabricated using materials that are regarded as highly biocompatible. It is also possible that unanticipated reactivity results due to the novel insertion method. Finally, since alterations in electrode design characteristics have the potential to influence not only the tissue response to implants, but also the electrical and mechanical performance of the devices, it will be critical to move towards standardization of electrophysiological metrics of success (longevity, signal-to-noise ratio, the number of units, site impedance, etc) in the context of biocompatibility studies.

The combination of new federal funding initiatives, commercial ventures, and explosive growth in the number of medical applications for implanted electrode arrays has produced a groundswell of innovation in neurotechnology in recent years. However, many of these technologies have not achieved broad-based dissemination in the field, confining their impact to a few selected laboratories. A notable exception to this rule is the ‘Neuropixels’ array, which has become more broadly available recently [48]. However, many laboratories may not have the capabilities, funding, or motivation to support the broad-based dissemination of their novel device designs to the field. Likewise, modifying electrodes with polymer coatings, biologics, topographical cues [137, 148] and related approaches often remains within the purview of the specific lab originating the technique. With respect to surface coatings, rapid degradation calls for the long-term characterization of the *in vivo* effects of these materials in the brain [140, 141, 144, 149]. Corroborating results across laboratories should be a central focus of efforts in the field, in order to more systematically validate which designs produce improved tissue integration reproducibly. The need to standardize benchmarks for success goes hand-in-hand with identifying appropriate biomarkers for effective device-tissue integration.

5. Concluding remarks

Devices implanted in the brain often simultaneously adopt different biomaterials, unique device architectures, and varying feature sizes within each design. As each lab adopts their own strategies and approaches, the field begins to fragment in a way that makes it difficult to empirically determine which device elements generate the most stable and biocompatible chronic interfaces. Additionally, the analysis of biocompatibility is often limited to neuronal density and glial scar analyses, and in some cases, neglected almost entirely. Neural interfaces have recently gained popularity in private industries, potentially broadening the accessibility of neurotechnology to the public. As such, it is increasingly important to rationally design devices which maximize safety and efficacy, including a fair assessment of performance relative to user expectations. Biological boundaries intrinsically create limitations to the design space of next generation electrode arrays. It is important to understand, define, and work within these limits to create devices with an optimized combination of performance and biocompatibility. New approaches to assess biocompatibility using a broader arsenal of technologies, including the analysis of gene expression, will create new avenues to assess biocompatibility in neurons and glia at the tissue interface. Likewise, standardizing approaches, repeating results across laboratories, and performing systematic studies of the effects of device attributes on tissue response will be essential to move the field toward the rational design of seamlessly-integrated electrodes.

Acknowledgments

The authors thank John Seymour for his helpful feedback, Nick Heelan and Kathleen Williams for their helpful review of table references, and Bailey Winter and Shardul Deolekar for early discussions regarding the article concept EKP, CHT, and TER are funded by the National Institutes of Health (1R01NS10745101A1) and the Departments of Biomedical Engineering and Electrical/Computer Engineering at Michigan State University.

ORCID iDs

Cort H Thompson  <https://orcid.org/0000-0001-6111-3488>

Paras R Patel  <https://orcid.org/0000-0001-6146-718X>

Wen Li  <https://orcid.org/0000-0002-6862-8561>

References

- [1] Laxton A W *et al* 2010 A phase I trial of deep brain stimulation of memory circuits in Alzheimer's disease *Ann. Neurol.* **68** 521–34
- [2] Kuhn J *et al* 2015 Deep brain stimulation of the nucleus basalis of Meynert in Alzheimer's dementia *Mol. Psychiatry* **20** 353–60
- [3] Quinn E J *et al* 2015 Beta oscillations in freely moving Parkinson's subjects are attenuated during deep brain stimulation *Mov. Disord.* **30** 1750–8
- [4] Grahn P J *et al* 2014 A neurochemical closed-loop controller for deep brain stimulation: toward individualized smart neuromodulation therapies *Frontiers Neurosci.* **8** 169
- [5] Crowell A L, Riva-Posse P, Garlow S J and Mayberg H S 2014 Toward an understanding of the neural circuitry of major depressive disorder through the clinical response to deep brain stimulation of different anatomical targets *Curr. Behav. Neurosci. Rep.* **1** 55–63
- [6] Whiting D M *et al* 2013 Lateral hypothalamic area deep brain stimulation for refractory obesity: a pilot study with preliminary data on safety, body weight, and energy metabolism *J. Neurosurg.* **119** 56–63
- [7] Ho A L *et al* 2015 Deep brain stimulation for obesity: rationale and approach to trial design *Neurosurg. Focus* **38** E8
- [8] Rotsides J and Mammis A 2013 The use of deep brain stimulation in Tourette's syndrome *Neurosurg. Focus* **35** E4
- [9] Moore D R and Shannon R V 2009 Beyond cochlear implants: awakening the deafened brain *Nat. Neurosci.* **12** 686–91
- [10] Lim H H and Lenarz T 2015 Auditory midbrain implant: research and development towards a second clinical trial *Hear. Res.* **322** 212–23
- [11] Lewis P M, Ackland H M, Lowery A J and Rosenfeld J V 2015 Restoration of vision in blind individuals using bionic devices: a review with a focus on cortical visual prostheses *Brain Res.* **1595** 51–73
- [12] Peters H T, Edwards D J, Wortman-Jutt S and Page S J 2016 Moving forward by stimulating the brain: transcranial direct current stimulation in post-stroke hemiparesis *Frontiers Hum. Neurosci.* **10** 8
- [13] Smit J V *et al* 2015 Deep brain stimulation in tinnitus: current and future perspectives *Brain Res.* **1608** 51–65
- [14] Shekhawat G S *et al* 2016 Intensity, duration, and location of high-definition transcranial direct current stimulation for tinnitus relief *Neurorehabil. Neural Repair* **30** 349–59
- [15] Hochberg L R *et al* 2006 Neuronal ensemble control of prosthetic devices by a human with tetraplegia *Nature* **442** 164–71
- [16] US FDA 2005 *NeuroPort™ Cortical Microelectrode Array System K042384* www.accessdata.fda.gov/scripts/cdrh/cfdocs/cfpmn/pmn.cfm?ID=K042384
- [17] Collinger J L *et al* 2013 High-performance neuroprosthetic control by an individual with tetraplegia *Lancet* **381** 557–64
- [18] Aflalo T *et al* 2015 Decoding motor imagery from the posterior parietal cortex of a tetraplegic human *Science* **348** 906–10
- [19] Bouton C E *et al* 2016 Restoring cortical control of functional movement in a human with quadriplegia *Nature* **533** 247–50
- [20] Sun F T, Morrell M J and Wharen R E 2008 Responsive cortical stimulation for the treatment of epilepsy *Neurotherapeutics* **5** 68–74
- [21] Rosin B *et al* 2011 Closed-loop deep brain stimulation is superior in ameliorating parkinsonism *Neuron* **72** 370–84
- [22] Perge J A *et al* 2013 Intra-day signal instabilities affect decoding performance in an intracortical neural interface system *J. Neural Eng.* **10** 036004
- [23] Prasad A and Sanchez J C 2012 Quantifying long-term microelectrode array functionality using chronic *in vivo* impedance testing *J. Neural Eng.* **9** 026028
- [24] McCreery D B, Yuen T G H, Agnew W F and Bullara L A 1997 A characterization of the effects on neuronal excitability due to prolonged microstimulation with chronically implanted microelectrodes *IEEE Trans. Biomed. Eng.* **44** 931–9
- [25] McCreery D B, Agnew W F and Bullara L A 2002 The effects of prolonged intracortical microstimulation on the excitability of pyramidal tract neurons in the cat *Ann. Biomed. Eng.* **30** 107–19
- [26] Polikov V S, Tresco P A and Reichert W M 2005 Response of brain tissue to chronically implanted neural electrodes *J. Neurosci. Methods* **148** 1–18
- [27] Salatino J W, Ludwig K A, Kozai T D Y and Purcell E K 2018 Glial responses to implanted electrodes in the brain *Nat. Biomed. Eng.* **2** 52

- [28] Salatino JW, Kale A P and Purcell E K 2019 Alterations in ion channel expression surrounding implanted microelectrode arrays in the brain Accepted (<https://doi.org/10.1101/518811>)
- [29] Salatino JW, Winter B M, Drazin M H and Purcell E K 2017 Functional remodeling of subtype-specific markers surrounding implanted neuroprostheses *J. Neurophysiol.* **118** 194–202
- [30] Eles J R, Vazquez A L, Kozai T D Y and Cui X T 2018 Biomaterials *in vivo* imaging of neuronal calcium during electrode implantation: spatial and temporal mapping of damage and recovery *Biomaterials* **174** 79–94
- [31] Goss-Varley M et al 2017 Microelectrode implantation in motor cortex causes fine motor deficit: implications on potential considerations to brain computer interfacing and human augmentation *Sci. Rep.* **7** 15254
- [32] Oberlaender M et al 2011 Three-dimensional axon morphologies of individual layer 5 neurons indicate cell type-specific intracortical pathways for whisker motion and touch *Proc. Natl Acad. Sci.* **108** 4188–93
- [33] Kubota Y 2014 Untangling GABAergic wiring in the cortical microcircuit *Curr. Opin. Neurobiol.* **26** 7–14
- [34] Wellman S M and Kozai T D Y 2018 Biomaterials *in vivo* spatiotemporal dynamics of NG2 glia activity caused by neural electrode implantation *Biomaterials* **164** 121–33
- [35] Zhang Y and Barres B A 2010 Astrocyte heterogeneity: an underappreciated topic in neurobiology *Curr. Opin. Neurobiol.* **20** 588–94
- [36] Buffo A, Rolando C and Ceruti S 2010 Astrocytes in the damaged brain: molecular and cellular insights into their reactive response and healing potential *Biochem. Pharmacol.* **79** 77–89
- [37] Liddelow S A et al 2017 Neurotoxic reactive astrocytes are induced by activated microglia *Nature* **541** 481–7
- [38] Biran R, Martin D C and Tresco P A 2005 Neuronal cell loss accompanies the brain tissue response to chronically implanted silicon microelectrode arrays *Exp. Neurol.* **195** 115–26
- [39] Hong G and Lieber C M 2019 Novel electrode technologies for neural recordings *Nat. Rev. Neurosci.* **20** 330–45
- [40] Cabrera L, Saddle C and Purcell E 2019 Neuroethical considerations of high-density electrode arrays *Nat. Biomed. Eng.* **3** 586–9
- [41] Collias J C and Manuelidis E E 1957 Histopathological changes produced by implanted electrodes in cat brains *J. Neurosurg.* **14** 302–28
- [42] Liu X et al 1999 Stability of the interface between neural tissue and chronically implanted intracortical microelectrodes *IEEE Trans. Rehabil. Eng.* **7** 315–26
- [43] Winslow B D and Tresco P A 2010 Quantitative analysis of the tissue response to chronically implanted microwire electrodes in rat cortex *Biomaterials* **31** 1558–67
- [44] Drake K L, Wise K D, Farraye J, Anderson D J and BeMent S L 1988 Performance of planar multisite microprobes in recording extracellular single-unit intracortical activity *IEEE Trans. Biomed. Eng.* **35** 719–32
- [45] Vetter R J, Williams J C, Hetke J F, Nunamaker E A and Kipke D R 2004 Chronic neural recording using silicon-substrate microelectrode arrays implanted in cerebral cortex *IEEE Trans. Biomed. Eng.* **51** 896–904
- [46] Henze D A et al 2000 Intracellular features predicted by extracellular recordings in the hippocampus *in vivo* *J. Neurophysiol.* **84** 390–400
- [47] Shobe J L, Claar L D, Parhami S, Bakhurin K I and Masmanidis S C 2015 Brain activity mapping at multiple scales with silicon microprobes containing 1024 electrodes *J. Neurophysiol.* **114** 2043–52
- [48] Jun J J et al 2017 Fully integrated silicon probes for high-density recording of neural activity *Nature* **551** 232–6
- [49] Mora Lopez C et al 2017 A neural probe with up to 966 electrodes and up to 384 configurable channels in 0.13 μm SOI CMOS *IEEE Trans. Biomed. Circuits Syst.* **11** 510–22
- [50] Nordhausen C T, Maynard E M and Normann R A 1996 Single unit recording capabilities of a 100 microelectrode array *Brain Res.* **726** 129–40
- [51] Normann R A, Maynard E M, Rousche P J and Warren D J 1999 A neural interface for a cortical vision prosthesis *Vision Res.* **39** 2577–87
- [52] Bhandari R, Negi S, Rieth L, Normann R A and Solzbacher F 2009 A novel masking method for high aspect ratio penetrating microelectrode arrays *J. Micromech. Microeng.* **19** 035004
- [53] Malaga K A et al 2016 Data-driven model comparing the effects of glial scarring and interface interactions on chronic neural recordings in non-human primates *J. Neural Eng.* **13** 016010
- [54] Serruya M D, Hatsopoulos N G, Paninski L, Fellows M R and Donoghue J P 2002 Instant neural control of a movement signal *Nature* **416** 141–2
- [55] Santhanam G, Ryu S I, Yu B M, Afshar A and Shenoy K V 2006 A high-performance brain–computer interface *Nature* **442** 4–7
- [56] Barrese J C et al 2013 Failure mode analysis of silicon-based intracortical microelectrode arrays in non-human primates *J. Neural Eng.* **10** 066014
- [57] Kim S-P, Simeral J D, Hochberg L R, Donoghue J P and Black M J 2008 Neural control of computer cursor velocity by decoding motor cortical spiking activity in humans with tetraplegia *J. Neural Eng.* **5** 455–76
- [58] Bullard A 2019 *Feasibility of Using the Utah Array for Long-Term Fully Implantable Neuroprosthesis Systems* (University of Michigan) (<https://doi.org/10.37171/0033-2909.126.1.78>)
- [59] Hochberg L R et al 2012 Reach and grasp by people with tetraplegia using a neurally controlled robotic arm *Nature* **485** 372–5
- [60] Gilja V et al 2015 Clinical translation of a high-performance neural prosthesis **21** 6–8
- [61] Ajiboye A B et al 2017 Restoration of reaching and grasping movements through brain-controlled muscle stimulation in a person with tetraplegia: a proof-of-concept demonstration *Lancet* **389** 1821–30
- [62] Maynard E M, Fernandez E and Normann R A 2000 A technique to prevent dural adhesions to chronically implanted microelectrode arrays *J. Neurosci. Methods* **97** 93–101
- [63] Simeral J D, Kim S-P, Black M J, Donoghue J P and Hochberg L R 2011 Neural control of cursor trajectory and click by a human with tetraplegia 1000 days after implant of an intracortical microelectrode array *J. Neural Eng.* **8** 025027
- [64] Kao J C et al 2017 A high-performance neural prosthesis incorporating discrete state selection with hidden markov models *IEEE Trans. Biomed. Eng.* **64** 935–45
- [65] Chestek C A et al 2011 Long-term stability of neural prosthetic control signals from silicon cortical arrays in rhesus macaque motor cortex **8** 045005
- [66] Nolte N F, Christensen M B, Crane P D, Skousen J L and Tresco P A 2015 BBB leakage, astrogliosis, and tissue loss correlate with silicon microelectrode array recording performance *Biomaterials* **53** 753–62
- [67] Cody P A, Eles J R, Lagenaur C F, Kozai T D Y Y and Cui X T T 2018 Unique electrophysiological and impedance signatures between encapsulation types: an analysis of biological Utah array failure and benefit of a biomimetic coating in a rat model *Biomaterials* **161** 117–28
- [68] Wachrathit K et al 2019 Biotic response to long-term implantation of neural electrodes in the mouse motor cortex *9th Int. IEEE EMBS Conf. Neural Eng. Res.* https://neuro.embs.org/files/2013/0627_FL.pdf
- [69] Caldwell R et al 2018 Neural electrode resilience against dielectric damage may be improved by use of highly doped silicon as a conductive material *J. Neurosci. Methods* **293** 210–25
- [70] Caldwell R et al 2019 Analytical characterization of Parylene-C degradation mechanisms on Utah arrays: evaluation of *in vitro* reactive accelerated aging model compared to multiyear *in vivo* implantation Accepted (<https://doi.org/10.1101/743831>)
- [71] Takmakov P et al 2015 Rapid evaluation of the durability of cortical neural implants using accelerated aging with reactive oxygen species *J. Neural Eng.* **12** 026003
- [72] Xie C et al 2015 Three-dimensional macroporous nanoelectronic networks as minimally invasive brain probes *Nat. Mater.* **14** 1286–92

- [73] Liu J et al 2015 Syringe-injectable electronics *Nat. Nanotechnol.* **10** 629–35
- [74] Schuhmann T G et al 2018 Syringe-injectable mesh electronics for stable chronic rodent electrophysiology *J. Vis. Exp.* 1–15
- [75] Schuhmann T G, Yao J, Hong G, Fu T-M M and Lieber C M 2017 Syringe-injectable electronics with a plug-and-play input/output interface *Nano Lett.* **17** 5836–42
- [76] Zhou T et al 2017 Syringe-injectable mesh electronics integrate seamlessly with minimal chronic immune response in the brain *Proc. Natl Acad. Sci. USA* **114** 5894–9
- [77] Yang X et al 2019 Bioinspired neuron-like electronics *Nat. Mater.* **18** 510–7
- [78] Trevathan J K et al 2019 An injectable neural stimulation electrode made from an in-body curing polymer/metal composite *Adv. Healthc. Mater.* **8** 584995
- [79] Xu H et al 2015 Design of a flexible parylene-based multi-electrode array for multi-region recording from the rat hippocampus *2015 37th Annual Int. Conf. of the IEEE Engineering in Medicine and Biology Society (IEEE)* pp 7139–42
- [80] Xu H et al 2017 Chronic multi-region recording from the rat hippocampus *in vivo* with a flexible Parylene-based multi-electrode array *2017 39th Annual Int. Conf. of the IEEE Engineering in Medicine and Biology Society (IEEE)* pp 1716–9
- [81] Hara S A et al 2016 Long-term stability of intracortical recordings using perforated and arrayed Parylene sheath electrodes *J. Neural Eng.* **13** 066020
- [82] Seymour J P and Kipke D R 2007 Neural probe design for reduced tissue encapsulation in CNS *Biomaterials* **28** 3594–607
- [83] Purcell E K, Seymour J P, Yandamuri S and Kipke D R 2009 *In vivo* evaluation of a neural stem cell-seeded prosthesis *J. Neural Eng.* **6** 026005
- [84] Purcell E K, Singh A and Kipke D R 2009 Alginate composition effects on a neural stem cell-seeded scaffold *Tissue Eng. C* **15** 541–50
- [85] Rousche P J et al 2001 Flexible polyimide-based intracortical electrode arrays with bioactive capability *IEEE Trans. Biomed. Eng.* **48** 361–71
- [86] Tooker A et al 2012 Optimization of multi-layer metal neural probe design *2012 Annual Int. Conf. of the IEEE Engineering in Medicine and Biology Society (IEEE)* pp 5995–8
- [87] Chung J E et al 2019 High-density, long-lasting, and multi-region electrophysiological recordings using polymer electrode arrays *Neuron* **101** 21–31.e5
- [88] Wei X et al 2018 Nanofabricated ultraflexible electrode arrays for high-density intracortical recording *Adv. Sci.* **5** 1700625
- [89] Hanson T L, Diaz-Botia C A, Kharazia V, Maharbiz M M and Sabes P N 2019 The ‘sewing machine’ for minimally invasive neural recording Accepted (<https://doi.org/10.1101/578542>)
- [90] Du Z J et al 2017 Ultrasoft microwire neural electrodes improve chronic tissue integration *Acta Biomater.* **53** 46–58
- [91] Yoshida Kozai T D et al 2012 Ultrasmall implantable composite microelectrodes with bioactive surfaces for chronic neural interfaces *Nat. Mater.* **11** 1065–73
- [92] Patel P R et al 2015 Insertion of linear 8.4 μm diameter 16 channel carbon fiber electrode arrays for single unit recordings *J. Neural Eng.* **12** 046009
- [93] Patel P R et al 2016 Chronic *in vivo* stability assessment of carbon fiber microelectrode arrays *J. Neural Eng.* **13** 066002
- [94] Kozai T D Y Y, Jaquins-Gerstl A S, Vazquez A L, Michael A C and Cui X T 2015 Brain tissue responses to neural implants impact signal sensitivity and intervention strategies *ACS Chem. Neurosci.* **6** 48–67
- [95] Rusinek C A et al 2018 All-diamond microfiber electrodes for neurochemical analysis *J. Electrochem. Soc.* **165** G3087–92
- [96] Szarowski D H H et al 2003 Brain responses to micro-machined silicon devices *Brain Res.* **983** 23–35
- [97] Lee H C et al 2017 Histological evaluation of flexible neural implants; flexibility limit for reducing the tissue response? *J. Neural Eng.* **14** 036026
- [98] Stiller A et al 2018 A meta-analysis of intracortical device stiffness and its correlation with histological outcomes *Micromachines* **9** 443
- [99] Shen F et al 2006 Modified bilston nonlinear viscoelastic model for finite element head injury studies *J. Biomech. Eng.* **128** 797–801
- [100] Luan L et al 2017 Ultraflexible nanoelectronic probes form reliable, glial scar-free neural integration *Sci. Adv.* **3**
- [101] Stewart D C, Rubiano A, Dyson K and Simmons C S 2017 Mechanical characterization of human brain tumors from patients and comparison to potential surgical phantoms *PLoS One* **12** e0177561
- [102] Lippert S A, Rang E M and Grimm M J 2004 The high frequency properties of brain tissue *Biorheology* **41** 681–91
- [103] Rashid B, Destrade M and Gilchrist M D 2014 Mechanical characterization of brain tissue in tension at dynamic strain rates *J. Mech. Behav. Biomed. Mater.* **33** 43–54
- [104] Tamura A, Hayashi S, Watanabe I, Nagayama K and Matsumoto T 2007 Mechanical characterization of brain tissue in high-rate compression *J. Biomech. Sci. Eng.* **2** 115–26
- [105] Jin X, Zhu F, Mao H, Shen M and Yang K H 2013 A comprehensive experimental study on material properties of human brain tissue *J. Biomech.* **46** 2795–801
- [106] Luque T, Kang M S, Schaffer D V and Kumar S 2016 Microelastic mapping of the rat dentate gyrus *R. Soc. Open Sci.* **3** 150702
- [107] Green M, Bilstone L and Sinkus R 2008 *In vivo* brain viscoelastic properties measured by magnetic resonance elastography *NMR Biomed.* **21** 755–64
- [108] Vappou J et al 2007 Magnetic resonance elastography compared with rotational rheometry for *in vitro* brain tissue viscoelasticity measurement *Magn. Reson. Mater. Phys. Biol. Med.* **20** 273–8
- [109] Pogoda K et al 2014 Compression stiffening of brain and its effect on mechanosensing by glioma cells *New J. Phys.* **16** 075002
- [110] Atay S M, Kroenke C D, Sabet A and Bayly P V 2008 Measurement of the dynamic shear modulus of mouse brain tissue *in vivo* by magnetic resonance elastography *J. Biomech. Eng.* **130** 021013
- [111] Chauvet D et al 2015 *In vivo* measurement of brain tumor elasticity using intraoperative shear wave elastography *Ultraschall der Medizin—Eur. J. Ultrasound* **37** 584–90
- [112] Taylor Z and Miller K 2004 Reassessment of brain elasticity for analysis of biomechanisms of hydrocephalus *J. Biomech.* **37** 1263–9
- [113] Nakod P S, Kim Y and Rao S S 2018 Biomimetic models to examine microenvironmental regulation of glioblastoma stem cells *Cancer Lett.* **429** 41–53
- [114] Fomchenko E I and Holland E C 2006 Mouse models of brain tumors and their applications in preclinical trials *Clin. Cancer Res.* **12** 5288–97
- [115] Budday S et al 2017 Mechanical characterization of human brain tissue *Acta Biomater.* **48** 319–40
- [116] Lacour S P, Courtine G and Guck J 2016 Materials and technologies for soft implantable neuroprostheses *Nat. Rev. Mater.* **1** 16063
- [117] Kim D-H H, Abidian M and Martin D C 2004 Conducting polymers grown in hydrogel scaffolds coated on neural prosthetic devices *J. Biomed. Mater. Res.* **71A** 577–85
- [118] Capadona J R, Tyler D J, Zorman C A, Rowan S J and Weder C 2012 Mechanically adaptive nanocomposites for neural interfacing *MRS Bull.* **37** 581–9
- [119] Green R and Abidian M R 2015 Conducting polymers for neural prosthetic and neural interface applications *Adv. Mater.* **27** 7620–37
- [120] Hess A E et al 2011 Development of a stimuli-responsive polymer nanocomposite toward biologically optimized, MEMS-based neural probes *J. Micromech. Microeng.* **21** 054009
- [121] Nguyen J K et al 2014 Mechanically-compliant intracortical implants reduce the neuroinflammatory response *J. Neural Eng.* **11** 056014
- [122] Capadona J R et al 2008 Stimuli-responsive polymer nanocomposites inspired by the sea cucumber dermis *Science* **319** 1370–4

- [123] Ware T *et al* 2013 Thiol-ene/acrylate substrates for softening intracortical electrodes *J. Biomed. Mater. Res. B* **102** 1–11
- [124] Tien L W *et al* 2013 Silk as a multifunctional biomaterial substrate for reduced glial scarring around brain-penetrating electrodes *Adv. Funct. Mater.* **23** 3185–93
- [125] Kim D-H *et al* 2010 Dissolvable films of silk fibroin for ultrathin conformal bio-integrated electronics *Nat. Mater.* **9** 511–7
- [126] Subbaroyan J, Martin D C and Kipke D R 2005 A finite-element model of the mechanical effects of implantable microelectrodes in the cerebral cortex *J. Neural Eng.* **2** 103–13
- [127] Biran R, Martin D C and Tresco P A 2007 The brain tissue response to implanted silicon microelectrode arrays is increased when the device is tethered to the skull *J. Biomed. Mater. Res. A* **82A** 169–78
- [128] Thelin J *et al* 2011 Implant size and fixation mode strongly influence tissue reactions in the CNS *PLoS One* **6**
- [129] Harnett E M, Alderman J and Wood T 2007 The surface energy of various biomaterials coated with adhesion molecules used in cell culture *Colloids Surf. B* **55** 90–7
- [130] Richardson R R, Miller J A and Reichert W M 1993 Polyimides as biomaterials: preliminary biocompatibility testing *Biomaterials* **14** 627–35
- [131] Chang T Y *et al* 2007 Cell and protein compatibility of Parylene-C surfaces *Langmuir* **23** 11718–25
- [132] Weisenberg B A and Mooradian D L 2002 Hemocompatibility of materials used in microelectromechanical systems: platelet adhesion and morphology *in vitro* *J. Biomed. Mater. Res.* **60** 283–91
- [133] Mammadov B, Sever M, Guler M O and Tekinay A B 2013 Neural differentiation on synthetic scaffold materials *Biomater. Sci.* **1** 1119
- [134] Yang K-H and Narayan R J 2019 Biocompatibility and functionalization of diamond for neural applications *Curr. Opin. Biomed. Eng.* **10** 60–8
- [135] Farrukh A, Zhao S and del Campo A 2018 Microenvironments designed to support growth and function of neuronal cells *Frontiers Mater.* **5** 1–22
- [136] Vensi Basso J M, Yurchenko I, Simon M, Rizzo D J and Staii C 2019 Role of geometrical cues in neuronal growth *Phys. Rev. E* **99** 022408
- [137] Ereifej E S *et al* 2018 The neuroinflammatory response to nanopatterning parallel grooves into the surface structure of intracortical microelectrodes *Adv. Funct. Mater.* **28** 1–13
- [138] Kolarcik C L *et al* 2012 *In vivo* effects of L1 coating on inflammation and neuronal health at the electrode–tissue interface in rat spinal cord and dorsal root ganglion *Acta Biomater.* **8** 3561–75
- [139] Azemi E, Lagenaur C F and Cui X T 2011 The surface immobilization of the neural adhesion molecule L1 on neural probes and its effect on neuronal density and gliosis at the probe/tissue interface *Biomaterials* **32** 681–92
- [140] He W, McConnell G C, Schneider T M and Bellamkonda R V 2007 A novel anti-inflammatory surface for neural electrodes *Adv. Mater.* **19** 3529–33
- [141] Mercanzini A *et al* 2010 Controlled release nanoparticle-embedded coatings reduce the tissue reaction to neuroprostheses *J. Control. Release* **145** 196–202
- [142] Oakes R S, Polei M D, Skousen J L and Tresco P A 2018 An astrocyte derived extracellular matrix coating reduces astroglia surrounding chronically implanted microelectrode arrays in rat cortex *Biomaterials* **154** 1–11
- [143] Zhong Y and Bellamkonda R V 2007 Dexamethasone-coated neural probes elicit attenuated inflammatory response and neuronal loss compared to uncoated neural probes *Brain Res.* **1148** 15–27
- [144] Wadhwa R, Lagenaur C F and Cui X T 2006 Electrochemically controlled release of dexamethasone from conducting polymer polypyrrole coated electrode *J. Control. Release* **110** 531–41
- [145] Abidian M R and Martin D C 2009 Multifunctional nanobiomaterials for neural interfaces *Adv. Funct. Mater.* **19** 573–85
- [146] Harris J P *et al* 2011 Mechanically adaptive intracortical implants improve the proximity of neuronal cell bodies *J. Neural Eng.* **8** 066011
- [147] Michelson N J *et al* 2018 Multi-scale, multi-modal analysis uncovers complex relationship at the brain tissue-implant neural interface: new emphasis on the biological interface *J. Neural Eng.* **15** 033001
- [148] Thompson C H, Zoratti M J, Langhals N B and Purcell E K 2016 Regenerative electrode interfaces for neural prostheses *Tissue Eng. B* **22** 125–35
- [149] Guo T *et al* 2018 Three dimensional extrusion printing induces polymer molecule alignment and cell organization within engineered cartilage *J. Biomed. Mater. Res. A* **106** 2190–9
- [150] Gardella J A and Hercules D M 1980 Static secondary ion mass spectrometry of polymer systems *Anal. Chem.* **52** 226–32
- [151] Wang H and Chu P K 2013 Surface characterization of biomaterials *Characterization of Biomaterials* (Amsterdam: Elsevier) ch 4 pp 105–74
- [152] Kook G, Lee S, Lee H, Cho I-J and Lee H 2016 Neural probes for chronic applications *Micromachines* **7** 179
- [153] Seymour J P, Langhals N B, Anderson D J and Kipke D R 2011 Novel multi-sided, microelectrode arrays for implantable neural applications *Biomed. Microdevices* **13** 441–51
- [154] Brinen J S and Melera A 1972 Electron spectroscopy for chemical analysis (ESCA) studies on catalysts. Rhodium on charcoal *J. Phys. Chem.* **76** 2525–6
- [155] Pijolat M and Hollinger G 1981 New depth-profiling method by angular-dependent x-ray photoelectron spectroscopy *Surf. Sci.* **105** 114–28
- [156] Eles J R *et al* 2017 Neuroadhesive L1 coating attenuates acute microglial attachment to neural electrodes as revealed by live two-photon microscopy *Biomaterials* **113** 279–92
- [157] Ludwig K A, Uram J D, Yang J, Martin D C and Kipke D R 2006 Chronic neural recordings using silicon microelectrode arrays electrochemically deposited with a poly(3,4-ethylenedioxythiophene) (PEDOT) film *J. Neural Eng.* **3** 59–70
- [158] Cui X and Martin D C 2003 Electrochemical deposition and characterization of poly(3,4-ethylenedioxythiophene) on neural microelectrode arrays *Sensors Actuators B* **89** 92–102
- [159] Bezuidenhout D *et al* 2013 Covalent incorporation and controlled release of active dexamethasone from injectable polyethylene glycol hydrogels *J. Biomed. Mater. Res. A* **101A** 1311–8
- [160] Kato Y, Saito I, Hoshino T, Suzuki T and Mabuchi K 2006 Preliminary study of multichannel flexible neural probes coated with hybrid biodegradable polymer 2006 *Int. Conf. of the IEEE Eng. Med. Biol. Soc. (IEEE)* pp 660–3